Applied Catalysis B: Environmental 115–116 (2012) 53–62

Contents lists available at SciVerse ScienceDirect

Applied Catalysis B: Environmental

journal homepage: www.elsevier.com/locate/apcatb

MO_x (M = Mn, Fe, Ni or Cr) improved supported Co_3O_4 catalysts on ceria–zirconia nanoparticulate for CO preferential oxidation in H_2-rich gases

Zhongkui Zhao [a,b,*], Xiaoli Lin [a], Ronghua Jin [a], Guiru Wang [a], Turghun Muhammad [b]

[a] State Key Laboratory of Fine Chemicals, Department of Fine Chemicals, School of Chemical Engineering, Dalian University of Technology, 2 Linggong Road, Dalian 116024, China
[b] Key Laboratory of Oil & Gas Fine Chemicals, Ministry of Education & Xinjiang Uyghur Autonomous Region, Xinjiang University, Urumqi, Xinjiang 830046, China

ARTICLE INFO

Article history:
Received 8 September 2011
Received in revised form
30 November 2011
Accepted 1 December 2011
Available online 9 December 2011

Keywords:
CO preferential oxidation
MnO_x modification
Ceria–zirconia
Co-Mn interaction
PEM fuel cell

ABSTRACT

This approach dealt with the modification of our developed $Co_3O_4/Ce_{0.85}Zr_{0.15}O_2$ catalysts with transition metal oxides MO_x (M = Mn, Fe, Ni or Cr) for CO preferential oxidation (CO PROX) in H_2-rich gases. Results showed that just MnO_x modification remarkably broadened the temperature window of 100% CO conversion, also better than those in the report about Co-Mn composite catalysts from another research group. And even in the presence of H_2O and CO_2, the 175–225 °C temperature range for almost 100% CO conversion can be achieved over the optimized catalyst. Moreover, the addition of MnO_x significantly improved the catalytic activity and selectivity, which was dramatically better than those of the supported MnO_x or Co_3O_4 catalysts on ceria–zirconia nanoparticulate, indicating the existence of the remarkable Co-Mn synergistic effect. The MnO_x modified supported Co_3O_4 catalysts exhibited outstanding catalytic properties for CO PROX reaction, which was strongly dependent on the reducibility and dispersion of the active species affected by the Co/Mn atomic ratio and loading. The XRD and H_2-TPR techniques were performed to reveal the effect of structure–activity relationship on the catalytic properties. The analytic results presented that Co^{3+} was the main active species for CO PROX reaction, and the existence of Mn^{4+} and Mn^{3+} was also favorable to the reaction. The XRD and H_2-TPR characterization results affirmed the existence of strong interaction between Co and Mn, increasing the ratio of Co^{3+}/Co^{2+} resulted from the electron transfer between Co^{2+} and Mn^{4+}. Besides the improvement of Co_3O_4 dispersion and the enlargement of the Co^{3+}/Co^{2+} ratio through Co-Mn interaction, the addition of MnO_x could improve the stability of the ceria–zirconia support through the metal–support interaction. As a result, the CO selective oxidation reaction was efficiently improved. The 16 wt.%Co_3O_4-$MnO_x/Ce_{0.85}Zr_{0.15}O_2$ (Co/Mn = 8:1) could be a quite potential catalyst for eliminating trace CO from H_2-rich gases.

1. Introduction

The proton exchange membrane fuel cell (PEMFC) is a promising electronic apparatus with the H_2 as fuel [1,2]. However, the H_2-rich stream obtained from such as biomass steam reforming usually still contains 0.5–1% of CO after the water gas shift reaction (WGS) and this residual CO can poison the anode of the PEMFC [3]. The acceptable CO content is below 10 ppm for Pt anode and below 100 ppm for CO-tolerant alloy anodes [4–6]. Among the popular methods for CO removal from the H_2-rich gases, CO preferential oxidation (CO PROX) reaction is considered to be the direct, promising and cost-effective one to clean the trace CO from H_2-rich gases, and the CO concentration could be decreased to the desired level which meets the requirement for the anode of the PEMFC [7–9].

Studies on the catalysts used for CO PROX reaction have become a hot topic in the catalysis research domain. The catalysts used for the CO PROX reaction are mainly divided into two categories. One is the noble metal based catalysts represented by Au [10–13] and Pt [14–17]. Moreover, Rh [18,19], Ru [20–22] and Ag [23] based materials are also on the list of the noble metal catalysts. In the typical temperature window of 80–250 °C (from the fuel cell operating temperature ~80 °C to the WGS operating temperature ~200–250 °C) [24,25], this type of catalysts has the high CO conversion and CO_2 selectivity at low temperature in the absence of CO_2 and H_2O. However, besides the 0.5–1% CO, there still contains 10–25% CO_2 and about 10% H_2O in the H_2-rich stream [26,27]. Therefore, the high tolerance of CO_2 and H_2O for the CO PROX reaction is also essential to the catalysts. For the noble metal based catalysts, the catalytic activity and selectivity decrease obviously in the presence of CO_2 and H_2O [8,10,14,27]. In other words, the CO_2 and H_2O tolerance of these catalysts need further

* Corresponding author at: State Key Laboratory of Fine Chemicals, Department of Fine Chemicals, School of Chemical Engineering, Dalian University of Technology, 2 Linggong Road, Dalian 116024, China. Tel.: +86 411 84986231; fax: +86 411 84986231.
E-mail addresses: zkzhao@dlut.edu.cn, zzkdlut@yahoo.com (Z. Zhao).

0926-3373/$ – see front matter © 2011 Elsevier B.V. All rights reserved.
doi:10.1016/j.apcatb.2011.12.001

improvement. On the other hand, the availability and the price of the noble metals are the other barriers to their popularization. As a result, the other type of catalysts represented by Cu and Co based non-precious metal catalysts for the CO PROX reaction have been developed rapidly [5,28]. The Cu-Ce based catalysts are the most popular system for this reaction [29–32], and the cobalt based catalysts are another research direction in these non-precious metals [4,24,33,34]. It was found that Co_3O_4 based catalysts have shown good low-temperature activity, selectivity and the H_2O resistance [4,35–41]. The other metals like Mn [6,42–46], Fe [9,47] and Ni [48] are usually used as the additives for the Cu and Co-based composite catalysts, but not individually used in the CO PROX reaction.

In our previous report, we found that Co_3O_4/NP-CeO_2-ZrO_2 prepared by a reverse microemulsion (RM)/incipient wetness impregnation (IWI) method had exhibited promising catalytic properties for CO PROX reaction, resulted from the combination effect of the highly dispersed cobalt oxide, the improvement in CeO_2 reducibility due to ZrO_2 incorporation in CeO_2 structures, and the strong cobalt oxide–support interaction [4]. In this paper, we prepared the modified cobalt oxide catalysts supported on ceria–zirconia nanoparticulate using the MO_x (M = Mn, Fe, Ni or Cr) as the additives. The purpose is to find the suitable additive to further improve the catalytic properties of the supported cobalt oxide catalysts, such as the catalytic activity, selectivity and the CO_2 and H_2O tolerance. Results show that the catalytic properties of the developed MnO_x modified Co_3O_4/NP-CeO_2-ZrO_2 catalyst for CO PROX reaction in this paper is dramatically better than those of the unmodified one, and even obviously better than those of the mesoporous Co_3O_4/CeO_2-ZrO_2 reported by our research group recently [49]. Moreover, the relationship between catalytic performance and catalyst nature, and the synergistic effect between the additives and active species have been studied.

2. Experimental

2.1. Catalysts preparation

The $Ce_{0.85}Zr_{0.15}O_2$ support was prepared by the RM method as our previous report [4]. In a typical synthesis, the microemulsion B was added to the microemulsion A dropwise accompanied with vigorous stirring. Herein, the microemulsion A was comprised of nitrate salt precursors of Ce and Zr (the aqueous phase), cyclohexane (the organic phase), NP-10 (the surfactant) and 1-hexanol (the co-surfactant); the microemulsion B was similar to A except that the aqueous phase was replaced by $NH_3{\cdot}H_2O$. The vigorous stirring kept for 10 h after the microemulsion B dropped into A. Then, the mixture was aged for 14 h at room temperature. After that, the resulting brown precipitate was filtered, washed with deionized water and following with ethanol, dried overnight at 105 °C, and then calcined at 450 °C in a muffle for 5 h. The modified catalysts were prepared by the IWI method. The impregnant was the aqueous solution containing both the cobalt nitrate and the transition metal nitrate in accordance with the established Co/M atomic ratio. Then the samples were dried overnight at 105 °C, and followed by being calcined in a muffle for 5 h at 450 °C. The loading was calculated based on the percentage of Co_3O_4 and MO_x (M = Mn, Fe, Ni or Cr).

2.2. Catalysts characterization

XRD patterns were obtained using the Rigaku Automatic X-ray Diffractometer (D/Max 2400) equipped with a Cu Kα source (λ = 1.5406 Å). And the patterns were collected from 5 to 80° at step width of 0.02°. The average crystalline size was estimated by the MDI Jade5 software based on the Scherrer Formula over multiple characteristic diffraction peaks [4,49]. H_2-TPR technique was performed to estimate the reducibility of the catalysts. 100 mg sample was placed in a quartz tube reactor in each measurement. After pretreatment in a 2.5 vol.% O_2 flow with 30 ml min^{-1} flow rate at 300 °C for 30 min (the Ar flow was used for pretreatment process of the spent catalysts), the sample was cooled to room temperature in an Ar flow (30 ml min^{-1}). Then, the 10 vol.% H_2/Ar was switched into the system, and the temperature was raised up from 50 to 800 °C at a rate of 10 °C min^{-1}. The signal of H_2 consumption was detected by a thermal conductivity detector (TCD). Before the flow into the TCD, the H_2O generated in the process was eliminated by a water trap.

2.3. Catalytic performance measurement

The catalytic performance measurement was carried out in a stainless steel, fixed bed continuous-flow reactor (6 mm O.D.) at the atmospheric pressure. In each test, 200 mg catalyst with the defined particle size (200–250 mesh) was loaded between two quartz wool plugs. The temperature was measured by K-type thermocouples and controlled by a PID controller (Xiamen Yudian). Before the catalytic reaction, the sample was pretreated at a rate of 10 °C min^{-1} from the room temperature to 300 °C in a 2.5 vol.% O_2 flow (30 ml min^{-1}), and kept for 30 min at 300 °C. The reaction mixture was switched into the system after the sample being cooled to room temperature in an Ar flow. The feed contained 1.0 vol.% O_2, 1.0 vol.% CO, 50 vol.% H_2 and the balance Ar, which is controlled by the mass flow controllers (Huibolong). The analysis of the feed and the effluent was performed using a gas chromatograph on-line equipped with a TCD and a flame ionized detector (FID). The mixture containing CO, O_2, H_2 and CO_2 was separated by combing the 5A molecular sieve and PPQ columns. The trace CO and CO_2 were detected by FID after being converted to methane by a methanation reactor (the CO and CO_2 gas chromatogram peaks can be clearly detected even if their concentration are less than 10 ppm), and O_2 detected by the TCD. The water vapor (10 vol.%) and CO_2 (10 vol.%) was introduced into the reaction mixture when we studied the effect of the H_2O and CO_2 on the catalytic properties (simulating the reformed gas). The effluent gas was firstly cooled by a condenser with the ice water as the coolant to remove the H_2O before the gas flowing into chromatographic columns. The gas hourly space velocity (GHSV) of 15,000 ml g^{-1} h^{-1} was used for all the cases. No methane was detected over our catalysts in the temperature range from 50 to 250 °C, which was consistent with the previous reports [4,24].

The CO conversion and the CO_2 selectivity were calculated on the basis of the CO and O_2 concentrations in the feed and the effluent ($[CO]_{in}$, $[CO]_{out}$, $[O_2]_{in}$ and $[O_2]_{out}$) [4,49]. The every point of the light-off curve is an average of the three runs at isothermal conditions. CO conversion and CO_2 selectivity (O_2 selectivity to CO_2) were calculated on the basis of the equations as follows:

$$\text{CO conversion} \quad \chi_{CO}(\%) = \frac{[CO]_{in} - [CO]_{out}}{[CO]_{in}} \times 100$$

$$\text{O}_2\text{ conversion} \quad \chi_{O_2}(\%) = \frac{[O_2]_{in} - [O_2]_{out}}{[O_2]_{in}} \times 100$$

$$\text{H}_2\text{ conversion} \quad \chi_{H_2}(\%) = 2 \times \frac{\chi_{O_2} \times [O_2]_{in} - 0.5 \times \chi_{CO} \times [CO]_{in}}{[H_2]_{in}} \times 100$$

$$\text{CO}_2\text{ selectivity} \quad S_{CO_2}(\%) = \frac{\chi_{CO}}{2 \times \chi_{O_2}} \times 100$$

3. Results and discussion

3.1. Modification effects of the transition metals

In our previous report [4], the ceria–zirconia nanocomposite supported cobalt oxides as CO PROX catalysts were developed and the support effect (the zirconium incorporation into CeO_2) was investigated. We found that the supported cobalt oxide catalyst over ceria–zirconia nanoparticulate exhibited the relatively high catalytic activity and stability for the CO PROX reaction, but the 100% CO conversion just reached at the higher temperature. Herein, the present paper was devoted to improving the catalytic properties of the developed Co-supported catalysts at lower temperature by adding the other transition metals as promoters (the 4:1 for Co/M). The loading of 16 wt.% was used on the basis of the previous studies in our research group. The reaction results are presented in Fig. 1.

As seen in Fig. 1(a), in the reaction temperature range of 50–250 °C, the CO conversion increases and then maintains at the maximum conversion with the temperature increasing up to 200 °C. Further increase in reaction temperature leads to the decrease in CO conversion, which can be ascribed to the competitive oxidation with H_2 in the feed [24,40]. The selectivity of O_2 to CO conversion is exhibited in Fig. 1(b). As the reaction temperature is increased, the decrease in CO_2 selectivity can be observed, which can be ascribed to the H_2 oxidation. The addition of MO_x (M = Mn, Fe, Ni or Cr) has a significant effect on the catalytic activity and selectivity for CO PROX reaction. Compared with the unmodified Co-supported catalyst, the remarkable higher catalytic activity can be observed on the MnO_x modified catalyst, while the obviously lower on NiO_x or CrO_x modified ones. The 100% CO conversion at the temperature range of 150–200 °C can be obtained over the MnO_x modified supported Co_3O_4 catalyst. Towards the FeO_x modified one, the higher CO conversion at the reaction temperature being less than 150 °C but lower at the reaction temperature over 150 °C can be observed. From Fig. 1(b), all of the modified Co-supported catalysts exhibit higher selectivity for CO PROX reaction than the unmodified catalyst.

The XRD and H_2-TPR techniques were employed to probe the reasons why the modification with MnO_x can significantly improve the catalytic properties of the supported Co_3O_4 catalyst for CO PROX reaction in excess H_2. The XRD patterns and H_2-TPR profiles of the MnO_x modified and unmodified supported Co_3O_4 catalysts are presented in Figs. S1 (see supporting information) and 2, respectively. The quantitative results of XRD are provided in Table 1.

The XRD technique can be employed to reveal the nature of the significant enhancing effect of MnO_x on the catalytic properties of the supported Co_3O_4 catalyst. The crystalline phases present in the modified and unmodified supported Co_3O_4 catalysts on the ceria–zirconia support were established via XRD technique, and the XRD patterns are presented in Fig. S1. The cubic phase Co_3O_4 is identified by a comparison with the corresponding JCPDS file (JCPDS 43-1003), besides cubic phase $Ce_xZr_{1-x}O_2$ based on JCPDS file (JCPDS 28-0271). No crystalline phase of MnO_x can be resolved

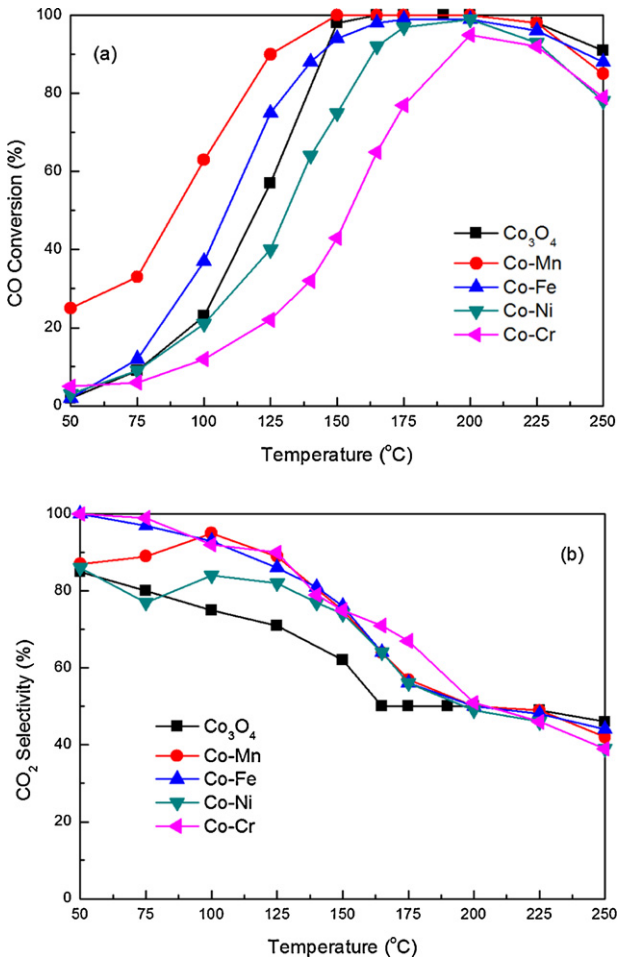

Fig. 1. Effect of the additives on CO conversion (a) and CO_2 selectivity (b) for CO PROX reaction catalyzed by the 16 wt.%Co_3O_4-MO_x/$Ce_{0.85}Zr_{0.15}O_2$ (M = Mn, Fe, Ni or Cr). Reaction conditions: GHSV = 15,000 ml h^{-1} g^{-1}, 1.0 vol.% CO, 1.0 vol.% O_2, 50 vol.% H_2 and balance Ar.

[50,51]. The addition of MnO_x results in the weaker and broader diffraction peaks of Co_3O_4 phase, suggesting the dispersity of Co_3O_4 should be improved. Probably the Co-Mn interaction leads to a loss of crystallinity [52]. The broadened diffraction peaks of the MnO_x modified catalyst represent the decrease in the average crystalline size [53]. The average crystalline size of Co_3O_4 for the two catalysts is estimated by the Scherrer equation, exhibiting the decrease from 14.9 to 13.1 nm while the MnO_x is introduced (Table 1). The improved dispersity of Co_3O_4 by the incorporation of MnO_x intensifies the CO PROX reaction. From Fig. S1, the shift of Co_3O_4 diffraction peaks to lower angles can be observed on the MnO_x modified supported Co_3O_4 catalyst, suggesting the expansion in Co_3O_4 unit cell. The similar phenomena can be found in the previous report [45], indicating that the $Mn_xCo_{3-x}O_4$ composite oxide phase is formed.

Table 1
XRD and TPR quantitative analysis results for the unmodified supported Co_3O_4 catalyst and the MnO_x modified supported catalysts with different Co/Mn atomic ratios.

Catalysts	Average crystallite size (nm)		H_2 consumption for the 1st peak (μmol/gcat)	Theoretical value for 1st peak[a]	Practical and theoretical ratio
	Co_3O_4	$Ce_{0.85}Zr_{0.15}O_2$			
Co:Mn = 4:1	13.1	5.2	537	914	0.6
Co:Mn = 8:1	10.4	5.2	664	803	0.8
Co:Mn = 12:1	13.0	5.3	710	759	0.9
Co_3O_4	14.9	5.8	579	664	0.9

[a] Calculated based on the H_2 uptake for the reduction of Co^{3+} and Mn^{4+} to Co^{2+} and Mn^{2+}, respectively.

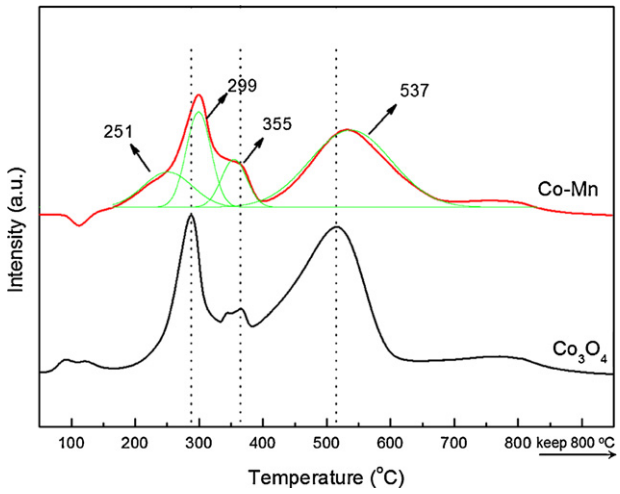

Fig. 2. H_2-TPR profiles of the MnO_x modified (Co/Mn ratio 4:1) and unmodified supported Co_3O_4 catalysts.

It can be identified that there can exist electron transfer between Co^{2+} and Mn^{4+} in the $Mn_xCo_{3-x}O_4$ composite oxide, and a partial Co^{2+} and Mn^{4+} may be transformed into Co^{3+} and Mn^{3+}/Mn^{2+}, respectively [45,52]. The lattice constants of Co_3O_4 unit cell for the MnOx modified and unmodified catalysts are 5.7324 and 5.6992 Å, respectively. The enlargement occurs due to the replacement of Co^{3+} (0.64 Å) in the matrix by Mn^{3+} (0.66 Å), and Co^{2+} (0.78 Å) by Mn^{2+} (0.80 Å) with a slight larger ion radius. The change of Co^{2+} to Co^{3+} results in the improved catalytic properties for CO PROX reaction.

From Fig. 2, the reduction peaks before 400 °C (1st peak) could be assigned to the reduction of cobalt oxide and MnO_x [52,54,55]. And the reduction peak above 400 °C (2nd peak) should contain the partial reduction of CeO_2, besides the reduction of Co^{2+} and Mn^{2+} to metal [6]. The two shoulders at the low and high temperature sides of the 1st peak clearly appear on the MnO_x modified supported Co_3O_4 catalyst, respectively. For further analysis, the 1st peak is resolved into three reduction peaks (251, 299 and 355 °C), which can be assigned to the reduction of the Mn^{4+}, Co^{3+}/Mn^{3+} and the interacted Co^{3+}/Mn^{3+} with support, respectively [52]. Whereas no shoulder at the low temperature side of 1st peak for the unmodified catalyst can be observed. The existence of Mn^{4+} and Mn^{3+} might be favorable for CO oxidation.

Based on the above analysis of the reaction and characterization results, it is confirmed that Co^{3+} is the main active species for CO PROX reaction, and the existence of Mn^{4+} and Mn^{3+} also enhances the reaction.

3.2. Effect of Co/Mn atomic ratio

From the analysis of the effect of the additives on the supported cobalt catalysts for CO PROX reaction, we concluded that the addition of MnO_x improved the catalytic properties for CO PROX reaction in excess H_2. In order to further improve the catalytic performance of supported Co_3O_4 catalyst, in this part we study the effect of Co/Mn atomic ratio on the catalytic properties for the CO PROX. And the reaction results are presented in Fig. 3.

From Fig. 3(a), we can see that the catalyst with MnO_x as the only active component exhibits the lowest CO conversion. The maximum CO conversion just reaches 93% at 175 °C. Then, compared with the unmodified supported Co_3O_4 catalyst, the Co_3O_4-MnO_x bicomponent catalysts have higher catalytic activity. From Fig. 3(b), we can clearly see that the addition of MnO_x also increases the selectivity for CO PROX reaction. The remarkable better catalytic

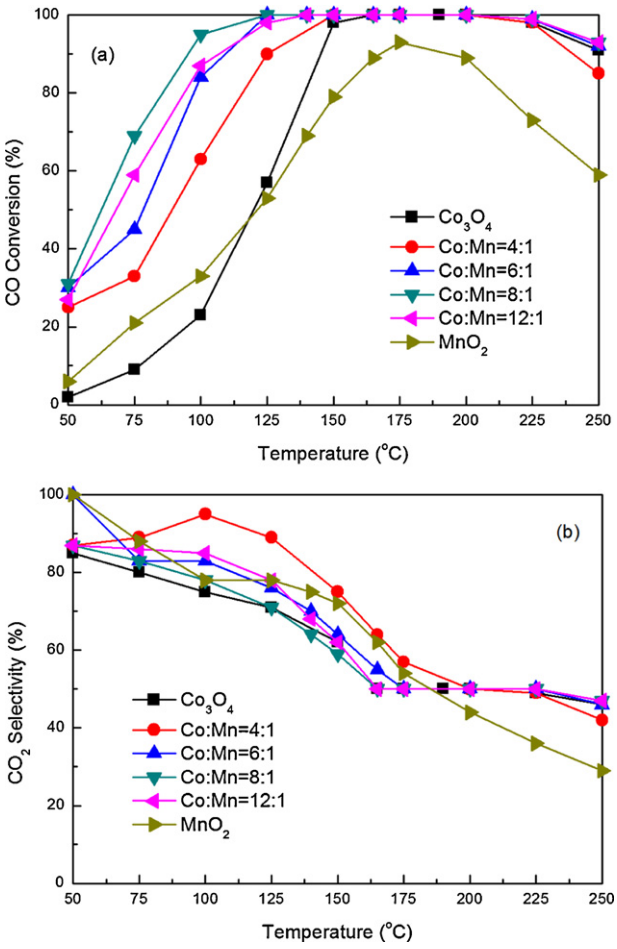

Fig. 3. Effect of the Co/Mn atomic ratio on CO conversion (a) and CO_2 selectivity (b) for CO PROX reaction catalyzed by 16 wt.%Co_3O_4-MnO_x/$Ce_{0.85}Zr_{0.15}O_2$. Reaction conditions: GHSV = 15,000 ml h^{-1} g^{-1}, 1.0 vol.% CO, 1.0 vol.% O_2, 50 vol.% H_2 and balance Ar.

properties of MnO_x modified supported Co_3O_4 catalysts than the supported Co_3O_4 or MnO_2 catalyst can be observed, indicating the existence of the clear synergistic effect between Co and Mn (how the synergistic effect to be produced would be revealed through analyzing the XRD and TPR characterization as followings). Moreover, we can also observe the catalytic properties to be dependent on the Co/Mn atomic ratio. Under the same reaction temperature, the activity and selectivity orders are 8:1 > 6:1 ~ 12:1 > 4:1 and 4:1 > 12:1 ~ 8:1 ~ 6:1, respectively. However, the order of selectivity at the lowest reaction temperatures for 100% CO conversion is 4:1 > 8:1 > 6:1 > 12:1 (remarkably more than that of unmodified catalyst). Further comparing the catalytic reaction results of the MnO_x modified supported Co_3O_4 catalysts with the Co/Mn atomic ratio of 8:1 and 4:1, we observe the obviously higher catalytic activity but slight lower CO_2 selectivity at the lowest temperature for 100% CO conversion over the modified catalyst with the Co/Mn atomic ratio of 8:1 than those over the other one. The above reaction results clearly indicate the MnO_x modified supported Co_3O_4 catalyst with 8:1 of Co/Mn atomic ratio has the best catalytic properties for CO PROX reaction in excess H_2. The four typical samples (the unmodified supported Co_3O_4 catalyst and the MnO_x modified catalysts with the Co/Mn atomic ratios of 4:1, 8:1 and 12:1) are chosen to further analyze the effect of Co/Mn atomic ratio on H_2 conversion and to reveal the structure–properties relationship of catalysts and the essential rules of Co-Mn interaction. Fig. 4 presents the H_2 conversion results of the unmodified and MnO_x modified supported Co_3O_4 catalysts with the Co/Mn atomic ratios of 4:1, 8:1 and 12:1.

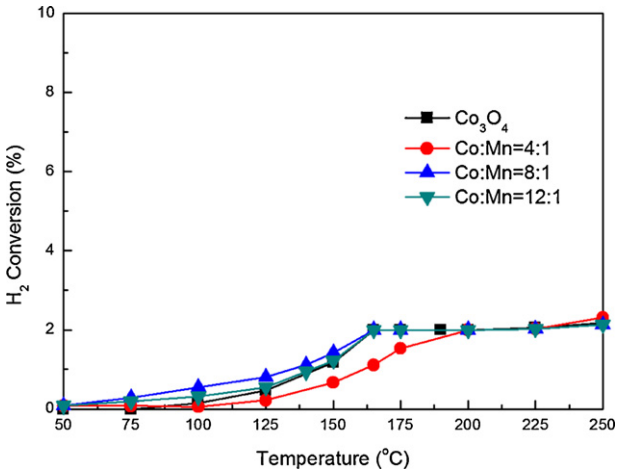

Fig. 4. H_2 conversion over the unmodified and MnO_x modified supported Co_3O_4 catalysts with the Co/Mn atomic ratios of 4:1, 8:1 and 12:1. Reaction conditions: GHSV = 15,000 ml h^{-1} g^{-1}, 1.0 vol.% CO, 1.0 vol.% O_2, 50 vol.% H_2 and balance Ar.

From Fig. 4, the order of H_2 conversion over the unmodified catalyst and the MnO_x modified catalyst with the Co/Mn atomic ratio of 8:1 and 12:1 is that: 8:1 > 12:1 > Co_3O_4 > 4:1. Among the MnO_x modified catalysts, only the sample with the Co/Mn ratio of 4:1 exhibits the slight lower catalytic activity for H_2 oxidation than the unmodified catalyst. Fortunately, the catalyst (Co/Mn = 4:1) exhibits the dramatically lower catalytic activity for CO oxidation than the other two modified catalysts, although higher than the unmodified catalyst. Due to the same loading (Co + Mn) being used for all the samples, there exists less cobalt species on the modified catalysts with more MnO_x incorporation into Co_3O_4. Correlated to the reaction results, we can safely say that the Co species can catalyze both CO and H_2 oxidation, but Mn species mainly enhance CO oxidation.

From above, the modified catalyst with optimum Co/Mn atomic ratio (8:1) has exhibited outstanding catalytic properties for CO PROX reaction in excess H_2, which might be resulted from the interaction between Co and Mn. Furthermore, the XRD and H_2-TPR experiments over the above four catalysts were performed to characterize the catalyst nature and reducibility, and therefore to reveal the rules of Co-Mn interaction.

The XRD patterns of the unmodified and the chosen MnO_x modified catalysts (Co:Mn = 4:1, 8:1 and 12:1) are presented in Fig. S2, and the average crystalline sizes of Co_3O_4 and $Ce_{0.85}Zr_{0.15}O_2$ phases are listed in Table 1.

In Fig. S2, the crystalline phases in the unmodified and MnO_x modified catalysts were identified by comparison with the corresponding JCPDS files (see them as above). Compared with the diffraction peaks of Co_3O_4 phase on the pattern of unmodified Co_3O_4 catalyst, the peaks on the MnO_x modified catalysts all become weaker and broader. The phenomena indicate the decreased average crystalline size of the cobalt oxide [45]. From Table 1, the average crystalline size of Co_3O_4 decreases in some degree as the different amount of MnO_x is introduced into the supported Co_3O_4 catalysts. Especially for the modified catalyst with Co/Mn ratio 8:1, the 10.4 nm of minimum average crystalline size can be observed. The phenomenon demonstrates the dispersion of Co_3O_4 is efficiently improved, which might be resulted from the interaction between Co and Mn. From Table 1, we also can see the lower average crystalline size of $Ce_{0.85}Zr_{0.15}O_2$ phase of the MnO_x modified catalysts than that of the unmodified catalyst, indicating the existence of the stabilization effect towards catalyst support led by the metal–support interaction. The stabilization effect also might improve the catalytic properties of support Co_3O_4 catalysts for CO PROX reaction. But this stabilization effect is independent of the Co/Mn atomic ratio. Therefore, the reason for the catalytic properties of supported Co_3O_4 catalysts being strongly dependent of Co/Mn atomic ratio should be mainly due to the Co-Mn interaction. Herein, the effect of Co/Mn atomic ratio on the Co_3O_4 crystalline phases would be further analyzed.

From Fig. S2, with respect to the XRD pattern of the unmodified catalyst, the diffraction peaks of Co_3O_4 slightly shifted to the low-angle direction for the MnO_x modified supported catalysts. This shift becomes clearer and clearer with the Co/Mn atomic ratio being decreased up to 8:1, but the further increase in MnO_x concentration leads to the shift being weaken. The phenomena definitely indicate the existence of the strong interaction between Co and Mn, and also the formation of $Mn_xCo_{3-x}O_4$ composite oxide phase [56,57]. As we described as above, the addition of MnO_x made some Co^{2+} transform to Co^{3+}, and meanwhile Mn^{4+} to Mn^{3+}/Mn^{2+}. The increased concentration in Co^{3+} improves the catalytic activity for CO and H_2 oxidation and selectivity of the modified supported Co_3O_4 catalysts, indicating the selective promotion effect of MnO_x incorporation towards the CO oxidation in excess H_2. Further increase in Mn concentration (Co/Mn from 8:1 to 4:1) may lead to the increase in Co^{3+}/Co^{2+} ratio. But the too large Mn concentration leads to the decrease in the total Co concentration since the same loading (Co + Mn) is adopted. The transfer of Co^{2+} to Co^{3+}, and Mn^{4+} to Mn^{3+}/Mn^{2+} can result in the enlargement in the unit cell constant, but the residual untransformed Mn^{4+} (0.60 Å) due to too large Mn concentration would lead to the decrease in unit cell constant. This could lead to the diffraction peaks of Co_3O_4 on the modified catalyst with 4:1 Co/Mn shift to the high-angle direction, compared with those on the modified one with 8:1 Co/Mn. As a result, the decrease in both CO and H_2 conversions can be observed. The optimum Co/Mn is required for CO PROX reaction, and the MnO_x modified supported Co_3O_4 catalyst with atomic ratio of 8:1 exhibits the better catalytic properties than those of the unmodified and the MnO_x modified catalysts with the inapposite Co/Mn. The above analysis further confirms the Co^{3+} is the main species for CO oxidation, and the Co-Mn synergistic effect can remarkably improve the catalytic properties of MnO_x modified supported Co_3O_4 catalysts for CO PROX reaction.

In order to further affirm the existence of the strong Co-Mn interaction in the MnO_x modified supported CO_3O_4 catalysts, the reducibility measurement was performed over the four typical catalysts. The H_2-TPR profiles and quantitative analysis results are presented in Fig. 5 and Table 1, respectively.

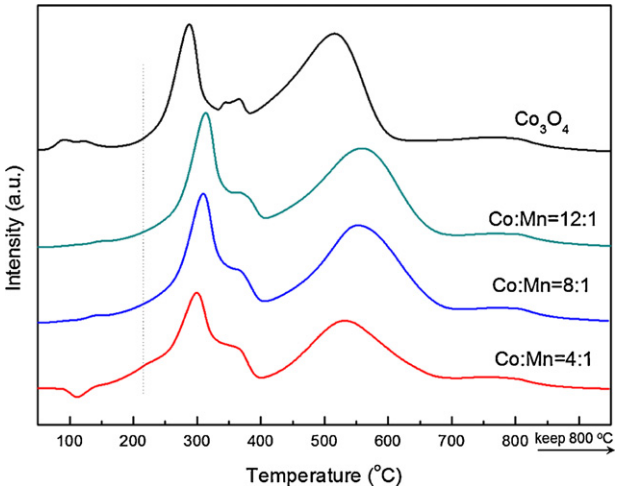

Fig. 5. H_2-TPR profiles of the 16 wt.%Co_3O_4-MnO_x/$Ce_{0.85}Zr_{0.15}O_2$ catalysts with different Co/Mn atomic ratios.

As is shown as above, the reduction peaks before 400 °C (1st peak) are assigned to the H_2 consumption for the reduction of Co^{3+} and MnO_x. And the reduction peaks above 400 °C (2nd peak) contain the partial reduction of CeO_2, Co^{2+} and Mn^{2+}. Based on the analysis results of XRD data, the 1st peak can be assigned to the reduction of the Mn^{4+}, Co^{3+}/Mn^{3+} and the interacted Co^{3+}/Mn^{3+} with support, respectively [52]. From our previous report [4], the 1st reduction peak corresponding to the reducible Co^{3+} has the decisive effect on the CO PROX reaction. Compared with the profiles of the unmodified supported catalyst, the broad reduction peaks with a slight shift to higher temperature can be observed on the MnO_x modified catalysts. It suggests the existence of the strong interaction between Co and Mn. Herein, we compare the H_2 consumption for the 1st reduction peak (Table 1), and find that the H_2 uptake of the MnO_x modified catalysts is larger than that of the unmodified sample, except for the sample with 4:1 of Co/Mn. It further confirms that the incorporation of MnO_x increase the amount of reducible species, although the same loading being used. As a result, the two MnO_x modified catalysts (Co/Mn = 8:1 and 12:1) show the better catalytic activity and selectivity for CO PROX reaction than those of the unmodified catalysts. Moreover, as the Mn doping amount is increased (Co/Mn from 12:1 to 4:1), the decrease in the practical and theoretical H_2 uptake ratio can be observed, implying too many mount of MnO_x can weaken the reducibility of the catalysts. As a result, compared with the modified catalysts with 8:1 and 12:1 of Co/Mn, the modified one with 4:1 of Co/Mn exhibits the worse catalytic performance, and even the catalytic performance is worse than that of the unmodified one. Although the little decreased H_2 uptake of the modified catalyst with 8:1 of Co/Mn (compared with the one with 12:1 of Co/Mn) can be observed, the lower reduction temperature may allow it have better catalytic activity for CO PROX reaction. Correlated to the reaction results, the amount of the reducible species at low temperature (1st peak, before 400 °C) has a significant effect on the CO PROX reaction, and the optimal amount of additives is essential. Moreover, with the increase in Mn content, the shoulder peak at the low temperature sides of the 1st peak (assigned to the reduction of Mn^{4+}) becomes clearer and clearer, and the well-resolved reduction peak for Mn^{4+} can be observed on the H_2 consumption profile of the modified catalyst with 4:1 Co/Mn, further confirming the existence of the untransformed Mn^{4+}, which is accordant to the analysis results from the XRD patterns. Comparing the H_2 consumption of modified catalyst (Co/Mn = 4:1) with that of unmodified one, the increased H_2 consumption for 1st peak (assigned to the reduction of the reducible $Co^{3+}/Mn^{4+}/Mn^{3+}$) but decreased for 2nd one (assigned to the reducible Co^{2+}, Mn^{2+} and Ce^{4+}) can be observed. Correlated to the catalytic properties of the two catalysts, we may propose that the $Co^{3+}/Mn^{4+}/Mn^{3+}$ can efficiently catalyze the CO oxidation reaction, but Co^{2+}, Mn^{2+} and Ce^{4+} mainly for H_2 oxidation. From Fig. 5, it is interesting to see a small negative peak around 100 °C in the TPR profile, which may be due to the H_2 desorption of the absorbed H_2 on the surface of catalyst during the process of baseline balance [58].

In a word, due to the Co-Mn synergistic effect, besides the metal–support interaction, the supported Co_3O_4 catalyst modified with an optimum Mn content (Co/Mn = 8:1) exhibits outstanding catalytic properties for CO PROX in excess H_2. The loading effect would be investigated to further improve the catalytic properties of the MnO_x modified supported Co_3O_4 catalysts.

3.3. Effect of the loading

The effect of loading (Co + Mn, Co/Mn = 8:1) on the catalytic properties of MnO_x modified supported Co_3O_4 catalysts were further investigated, and the reaction results are presented in Fig. 6.

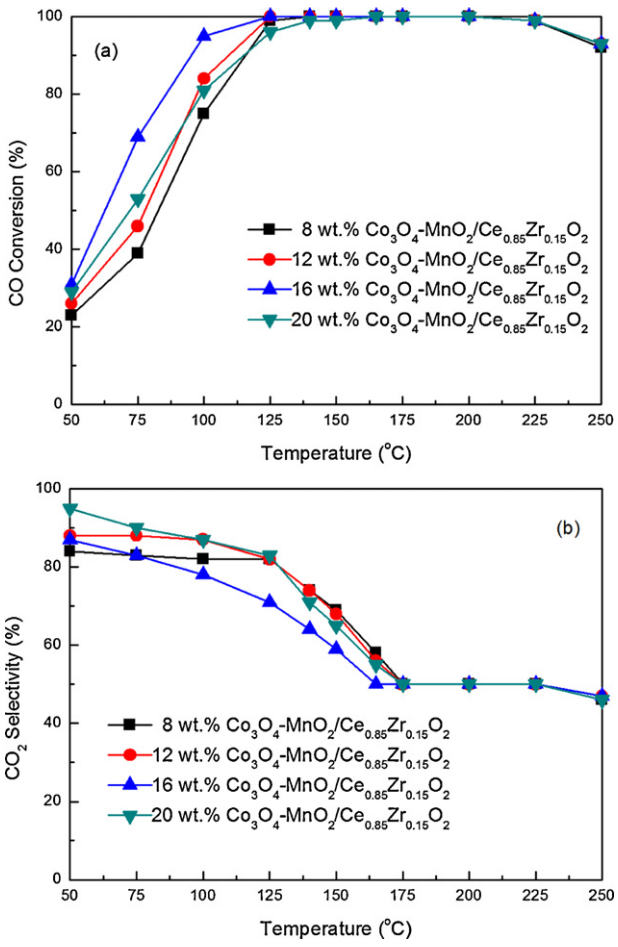

Fig. 6. Effect of the loading on CO conversion (a) and CO_2 selectivity (b) for CO PROX reaction catalyzed by MnO_x modified supported Co_3O_4 catalysts. Reaction conditions: GHSV = 15,000 ml h^{-1} g^{-1}, 1.0 vol.% CO, 1.0 vol.% O_2, 50 vol.% H_2 and balance Ar.

From Fig. 6, we can see that the MnO_x modified supported Co_3O_4 catalyst with the loading of 16 wt.% has exhibited excellent catalytic properties for CO PROX reaction. For the MnO_x modified supported Co_3O_4 catalysts with different loadings, the order of the CO conversion is as follows: 16 wt.% > 12 wt.% > 8 wt.% > 20 wt.%. Except for the catalyst with the loading of 20 wt.%, all the left can provide 100% CO conversion at 125–200 °C (almost 100% CO conversion in the range of 125–225 °C). From Fig. 6(b), only slight lower selectivity over the MnO_x modified catalyst with 16 wt.% loading than that of the others can be observed.

The XRD and the H_2-TPR techniques were employed to explore the reason why the CO conversion increases up to maximum, and then decrease, as the loading is continuously increased from 8 to 20 wt.%. Fig. 7 presents the XRD patterns of MnO_x modified supported Co_3O_4 catalysts with typically different loadings (8 wt.%, 16 wt.% and 20 wt.%).

From Fig. 7, no well-resolved diffraction peak corresponding Co_3O_4 phase on the catalyst with 8 wt.% loading can be observed, indicating the Co_3O_4 being highly dispersed. The diffraction peaks corresponding Co_3O_4 phase become stronger and narrower with the further increase in the loading up to 20 wt.%, implying the increase in average crystalline size. We estimate the average crystalline size of Co_3O_4 on the modified catalysts with the loading of 8, 16 and 20 wt.% by the Scherrer equation. The average crystalline size for the above three catalysts are 9.8, 10.4 and 13.2 nm, respectively. Correlated to reaction results, the amount of active species may be increased with the increase in loading, which is favorable

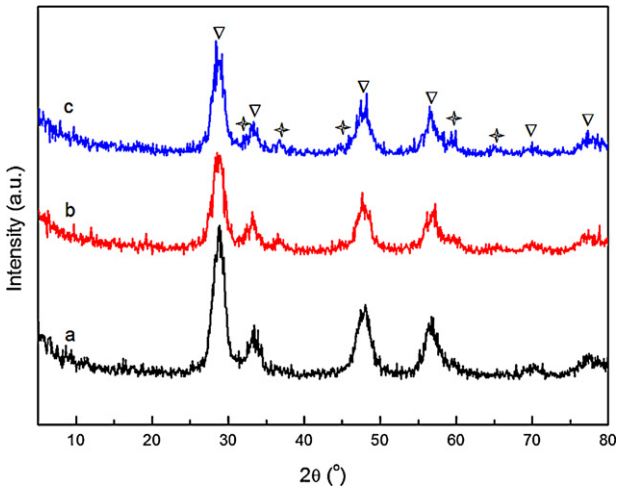

Fig. 7. XRD patterns of the MnO_x modified $Co_3O_4/Ce_{0.85}Zr_{0.15}O_2$ catalysts with different loadings (a) 8 wt.%; (b) 16 wt.% and (c) 20 wt.%. (▽) Fluorite-type cubic $Ce_xZr_{1-x}O_2$ composite oxide; (✧) cubic Co_3O_4.

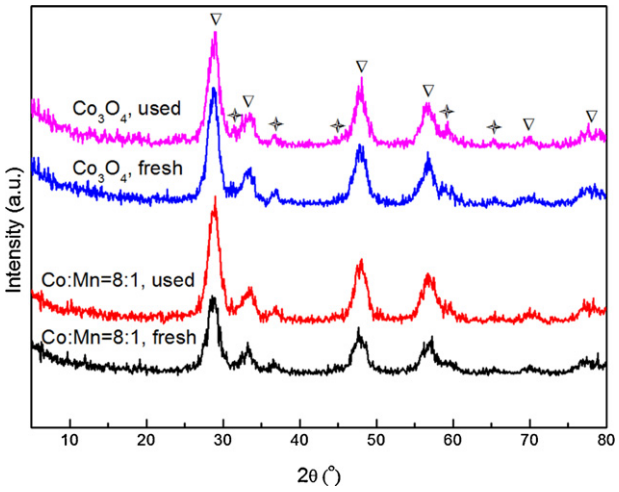

Fig. 9. XRD patterns of the fresh and used MnO_x modified/unmodified supported Co_3O_4 catalysts.

for the CO PROX reaction. But the too high loading may lead to the agglomeration of the active species, resulting in the poor dispersion. As a result, the continuous increase in loading from 8 to 20 wt.% cannot lead to the monotonous increase in CO conversion, and the catalyst with 16 wt.% loading demonstrates the highest catalytic activity for CO PROX reaction.

H_2-TPR measure can be used to investigate the reducibility of catalyst. Fig. 8 presents the H_2-TPR profiles of the MnO_x modified supported Co_3O_4 catalysts with typically different loadings (8 wt.%, 16 wt.% and 20 wt.%).

From Fig. 8, the increasing 1st peak area assigned to the reduction of $Co^{3+}/Mn^{4+}/Mn^{3+}$ can be observed as the loading is increased, which suggests that the amount of reducible species can be increased by increasing the loading of catalyst. The more reducible species are favorable for increasing the catalytic activity. Through the quantitative analysis, we find the increase in loading from 8 to 20 wt.% leads to the gradual decrease in the H_2 consumption per loading, implying the decrease in reducibility resulted from the increasing loading. From Fig. 8, the 1st reduction peak of the catalyst shifts to higher temperature as the loading is increased from 8 to 20 wt.%, suggesting the worse reducibility led by higher loading. From the XRD analysis results, the higher loading results in the worse dispersion, which is the reason why the worse reducibility can be observed on the catalyst with the higher loading. Based on the above, the optimum loading is required for the supported Co_3O_4 catalysts with excellent catalytic properties.

Since the CO PROX reaction is carried out in reducing condition, it is interesting to investigate the change for the spent catalyst, and also the effect of Mn addition on this change. Figs. 9 and 10 present the XRD patterns and TPR profiles of both the fresh and spent MnO_x modified and Unmodified supported cobalt oxide catalysts on the ceria–zirconia nanoparticulate, respectively.

From Fig. 9, compared with fresh samples, except for the slight sharpening in XRD peaks, no visible change can be observed, which suggests that no change in crystal phase but growing crystalline size take place. In comparison with the spent unmodified supported Co_3O_4 catalyst, the used MnO_x modified catalyst still has definitely smaller Co_3O_4 average crystalline size. This might be a reason for the MnO_x modified catalyst having better catalytic performance than the unmodified one.

The TPR experiments are employed to further investigate the change for the catalyst suffering the reduction atmosphere. From Fig. 10, compared with the fresh catalysts, both of the spent catalysts have a lower H_2 consumption at the reduction temperature before 400 °C (assigned to the reduction for the main active species), which can be ascribed to the reduction in the reduction

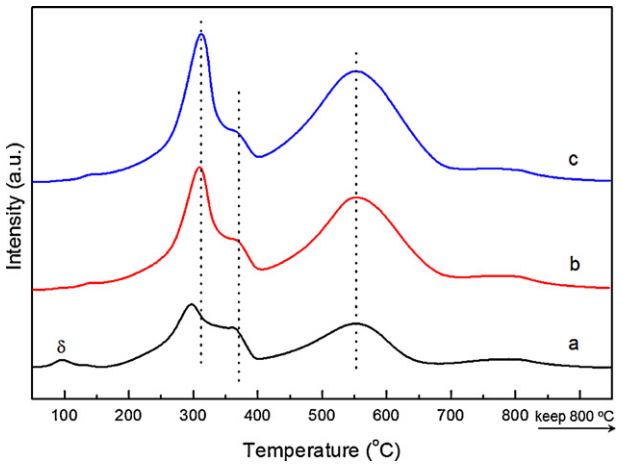

Fig. 8. H_2-TPR profiles of the MnO_x modified $Co_3O_4/Ce_{0.85}Zr_{0.15}O_2$ catalysts with different loadings (a) 8 wt.%; (b) 16 wt.% and (c) 20 wt.%.

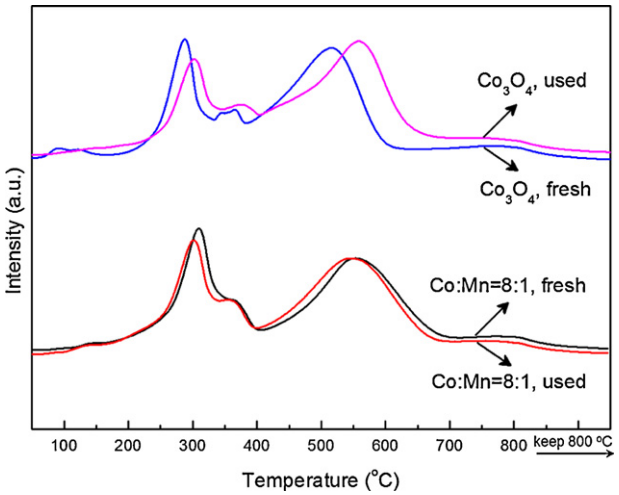

Fig. 10. TPR profiles of the fresh and used MnO_x modified/unmodified supported Co_3O_4 catalysts.

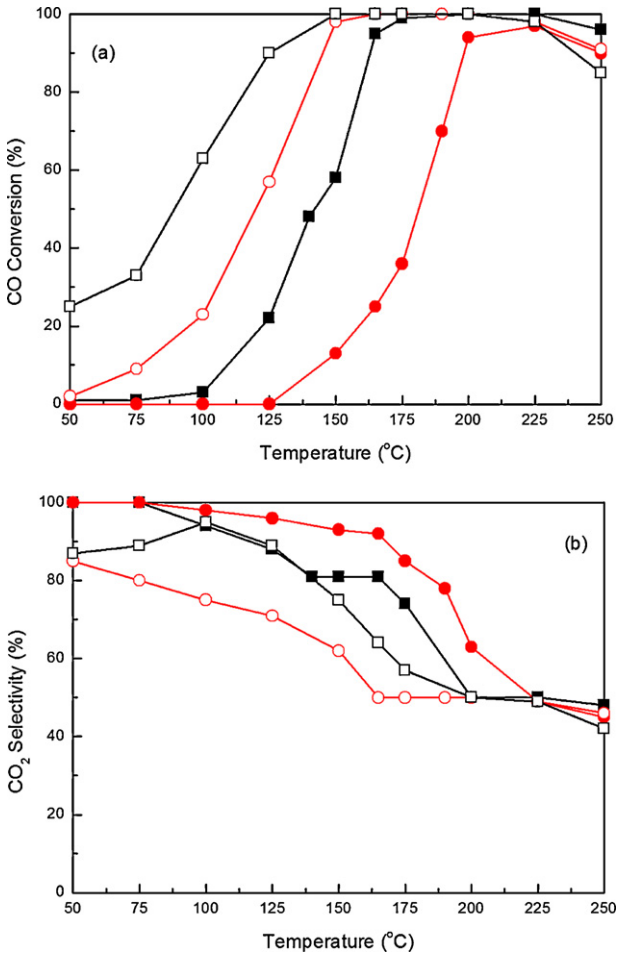

Fig. 11. CO conversion (a) and CO_2 selectivity (b) over the 16 wt.% Co_3O_4-$MnO_x/Ce_{0.85}Zr_{0.15}O_2$ (■/□) and 16 wt.% $Co_3O_4/Ce_{0.85}Zr_{0.15}O_2$ (●/○) for CO PROX reactions with (solid symbol)/without (open symbol) the H_2O and CO_2 in the feed. Reaction conditions: GHSV = 15,000 ml h^{-1} g^{-1}, 1.0 vol.% CO, 1.0 vol.% O_2, 50 vol.% H_2 and balance Ar (10 vol.% H_2O and 10 vol.% CO_2 are introduced into feed for investigating the effect of the H_2O and CO_2).

atmosphere in CO PROX reaction process. Furthermore, compared with the change for the unmodified catalyst, the change for the MnO_x modified one is negligible. This result demonstrates that the addition of MnO_x can improve the reduction tolerance of supported Co_3O_4 catalysts in the H_2-rich gas resulted from the strong interaction between Co and Mn, which allows the modified catalyst exhibiting much better catalytic performance in CO PROX reaction.

3.4. Effect of adding H_2O and CO_2

The H_2-rich gas obtained after the WGS reaction definitely contains H_2O and CO_2. Therefore, studying the catalytic properties of the catalysts for CO PROX reaction in the simulated syngas is more important. In this paper, we introduced 10 vol.% H_2O and 10 vol.% CO_2 into the H_2-rich gas to study the effect of H_2O and CO_2 on the unmodified supported Co_3O_4 catalyst and the MnO_x modified cobalt catalyst with the loading of 16 wt.% (Co/Mn = 8:1). The results are presented in Fig. 11.

From Fig. 11(a), over both the unmodified and the modified supported Co_3O_4 catalysts, the negative effect of the adding H_2O and CO_2 on the catalytic activity can be observed. Previous reports had ascribed the negative effect of H_2O to the blockage of the active sites by the water adsorbed [26,45,59,60]. It was also proposed that at low temperature the inhibiting effect of CO_2 mainly was ascribed to two reasons: the competitive adsorption of CO_2 with CO on the catalyst surface and the formation of the carbonates related to the interaction of CO_2 and the surface of ceria, which were considered to block the oxygen mobility on the support [31,55,59]. Furthermore, the less negative effect of H_2O and CO_2 over the MnO_x modified supported Co_3O_4 catalyst than over the unmodified sample, suggesting that the tolerance of H_2O and CO_2 is dramatically improved by the addition of MnO_x. We can see that in the presence of H_2O and CO_2, the maximum CO conversion over the unmodified catalyst is 97% at 225 °C, while the almost 100% CO conversion reaches at 175–225 °C (CO complete transformation at 200–225 °C) over the MnO_x modified catalyst. Moreover, compared with the results in the reference reported by the other group [45], the temperature range for CO complete transformation is broadened. From Fig. 11(b), no obvious decrease in selectivity over the MnO_x modified catalyst can be observed compared with the unmodified supported Co_3O_4 catalyst. From above, the MnO_x modified $Co_3O_4/Ce_{0.85}Zr_{0.15}O_2$ can be an excellent catalyst for CO PROX reaction in the simulated syngas.

3.5. Effect of time on stream

The stability of CO PROX reaction catalyst is essential for its practical utilization. The stability of our developed 16 wt.% Co_3O_4-$MnO_x/Ce_{0.85}Zr_{0.15}O_2$ (Co/Mn = 8:1) catalyst was investigated by performing CO PROX reaction experiment at 200 and 150 °C as a function of time on stream using a feed containing 1.0% CO, 1.0% O_2, 50% H_2, 10% H_2O, 10% CO_2, and Ar balance. Fig. 12 presents the CO conversion and CO_2 selectivity as a function of time on stream. The unmodified supported Co_3O_4 catalyst on $Ce_{0.85}Zr_{0.15}O_2$ was also included for comparison.

From Fig. 12, in the presence of CO_2 and H_2O, our 16 wt.% Co_3O_4-$MnO_x/Ce_{0.85}Zr_{0.15}O_2$ (Co/Mn = 8:1) catalyst exhibits good catalytic stability for CO PROX, and up to 1440 min, no obvious decrease in catalytic activity can be observed over MnO_x modified supported Co_3O_4 catalyst. However, the visible decrease in CO conversion can be observed over the unmodified supported Co_3O_4 catalyst, which might be ascribed to the reduction of Co^{3+} to Co^{2+} at the reduction atmosphere for CO PROX reaction and the growing crystalline size of Co_3O_4 affirmed by the XRD and TPR results of fresh and spent catalysts shown as above. From the above analysis in Figs. 9 and 10, the reaction atmosphere does not lead to an obvious change in Co^{3+} concentration and Co_3O_4 crystal size if the supported Co_3O_4 catalyst is modified by adding MnO_x. From Fig. 12, it can be observed that, although our fabricated 16 wt.% Co_3O_4-$MnO_x/Ce_{0.85}Zr_{0.15}O_2$ (Co/Mn = 8:1) catalyst exhibits good catalytic stability for CO PROX in the presence of CO_2 and H_2O up to 1440 min at high temperature (200 °C for CO full conversion), a visible decrease in both conversion and selectivity was observed while the reaction was performed at a low temperature (150 °C). From the above analysis in Fig. 10, the reduction atmosphere does not lead to an obvious change in Co^{3+} concentration. It is proposed that the noticeable decrease in catalytic activity might be mainly due to the existence of H_2O and CO_2 in the feed. Further work in our lab would be addressed to further improve the stability of catalyst for CO PROX in the presence of H_2O and CO_2 in the feed.

4. Conclusions

The MO_x (M = Mn, Fe, Ni or Cr) modified supported cobalt oxide catalysts on ceria–zirconia nanoparticulates were studied for CO PROX reaction in H_2-rich gases. The results showed that the addition of MnO_x could significantly enhance the catalytic properties of the supported Co_3O_4 catalysts for CO PROX reaction, and the appropriate Co/Mn atomic ratio and loading were essential to the modified catalysts. The tolerance of H_2O and CO_2 was also studied in

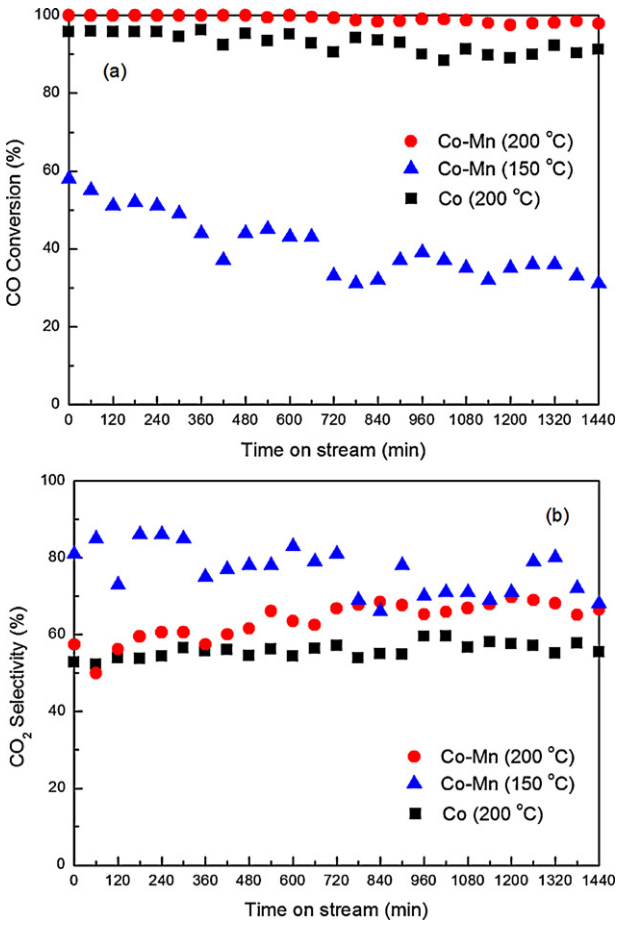

Fig. 12. Effect of the time on stream on CO conversion (a) and CO_2 selectivity (b) for CO PROX reactions in the presence of H_2O and CO_2 over the supported Co_3O_4-MnO_2 (Co/Mn ratio 8:1, at the 200 and 150 °C of reaction temperature) and Co_3O_4 catalysts (at the 200 °C of reaction temperature) on $Ce_{0.85}Zr_{0.15}O_2$ support, respectively. Reaction conditions: GHSV = 15,000 ml h^{-1} g^{-1}, 1.0 vol.% CO, 1.0 vol.% O_2, 10 vol.% H_2O, 10 vol.% CO_2, 50 vol.% H_2 and balance Ar.

the simulated syngas. Results showed that the MnO_x modified supported Co_3O_4 catalyst with the loading of 16 wt.% (Co/Mn = 8:1) had exhibited the excellent H_2O and CO_2 tolerance, and the almost 100% CO conversion could be obtained at 175–200 °C (and even completely transformation at the temperature range of 200–225 °C). The XRD and H_2-TPR characterization results suggested that Co^{3+} was the main active species for CO PROX reaction, and the existence of Mn^{4+} and Mn^{3+} was also favorable to the reaction. The reaction properties and characterization results of the MnO_x modified catalysts indicated the existence of the strong interaction between Co and Mn, resulted in electron transfer between Co^{2+} and Mn^{4+}. And a partial Co^{2+} and Mn^{4+} may be transformed into Co^{3+} and Mn^{3+}/Mn^{2+}, respectively. The reducibility of Co_3O_4 was efficiently improved due to the well dispersion on ceria–zirconia support resulted from the Co and Mn interaction. The stability of the ceria–zirconia support was also increased through the metal–support interaction. The TPR results for the fresh and spent catalysts demonstrate that the addition of MnO_x can improve the reduction tolerance of supported Co_3O_4 catalysts in the H_2-rich gas resulted from the strong interaction between Co and Mn. As a result, the addition of MnO_x remarkably improved the catalytic properties of supported Co_3O_4 catalysts on the $Ce_{0.85}Zr_{0.15}O_2$ nanoparticulate for CO PROX reaction in H_2-rich gases. In a word, the MnO_x modified supported Co_3O_4 sample with the appropriate Co/Mn atomic ratio and loading would be a very potential catalyst for CO PROX reaction in H_2-rich gases.

Acknowledgments

This work is financially supported by the National Natural Science Foundation of China (grant no. 20803006), and also sponsored by Key Laboratory of Oil & Gas Fine Chemicals, Ministry of Education & Xinjiang Uyghur Autonomous Region, Xinjiang University (grant no. XJDX0908-2011-10) and the Fundamental Research Funds for the Central Universities (DLUT).

Appendix A. Supplementary data

Supplementary data associated with this article can be found, in the online version, at doi:10.1016/j.apcatb.2011.12.001.

References

[1] D.T.S. Rosa, D.G. Pinto, V.S. Silva, R.A. Silva, C.M. Rangel, Int. J. Hydrogen Energy 32 (2007) 4350–4357.
[2] K.I. Lee, S.W. Lee, M.S. Park, C.N. Chu, Int. J. Hydrogen Energy 35 (2010) 11844–11854.
[3] J.R. Regalbuto, Science 325 (2009) 822–824.
[4] Z.K. Zhao, X.L. Lin, R.H. Jin, Y.T. Dai, G.R. Wang, Catal. Commun. 12 (2011) 1448–1451.
[5] E.D. Park, D. Lee, H.C. Lee, Catal. Today 139 (2009) 280–290.
[6] Q. Guo, Y. Liu, Appl. Catal. B: Environ. 82 (2008) 19–26.
[7] H. Zou, S. Chen, Z. Liu, W. Lin, Powder Technol. 207 (2011) 238–244.
[8] T. Tabakova, G. Avgouropoulos, J. Papavasiliou, M. Manzoli, F. Boccuzzi, K. Tenchev, F. Vindigni, T. Ioannides, Appl. Catal. B: Environ. 101 (2011) 256–265.
[9] Z. Lendzion-Bielun, M.M. Bettahar, S. Monteverdi, Catal. Commun. 11 (2010) 1137–1142.
[10] G. Avgouropoulos, M. Manzoli, F. Boccuzzi, T. Tabakova, J. Papavasiliou, T. Ioannides, V. Idakiev, J. Catal. 256 (2008) 237–247.
[11] T.A. Zepeda, A. Martinez-Hernández, R. Guil-López, B. Pawelec, Appl. Catal. B: Environ. 100 (2010) 450–462.
[12] S. Monyanon, S. Pongstabodee, A. Luengnaruemitchai, J. Power Sources 163 (2006) 547–554.
[13] G. Yi, H. Yang, B. Li, H. Lin, K. Tanaka, Y. Yuan, Catal. Today 157 (2010) 83–88.
[14] J.L. Ayastuy, A. Gil-Rodríguez, M.P. González-Marcos, M.A. Gutiérrez-Ortiz, Int. J. Hydrogen Energy 31 (2006) 2231–2242.
[15] S.K. Jain, E.M. Crabb, L.E. Smart, D. Thompsett, A.M. Steele, Appl. Catal. B: Environ. 89 (2009) 349–355.
[16] X. Yu, H. Li, S. Tu, J. Yan, Z. Wang, Int. J. Hydrogen Energy 36 (2011) 3778–3788.
[17] M. Schmal, R. Scheunemann, N.F.P. Ribeiro, J.F. Bengoa, Appl. Catal. A: Gen. 392 (2011) 1–10.
[18] C. Galletti, S. Specchia, G. Saracco, V. Specchia, Int. J. Hydrogen Energy 33 (2008) 3045–3048.
[19] G. Nikolaidis, T. Baier, R. Zapf, G. Kolb, V. Hessel, W.F. Maier, Catal. Today 145 (2009) 90–100.
[20] Y.H. Kim, E.D. Park, H.C. Lee, D. Lee, Appl. Catal. A: Gen. 366 (2009) 363–369.
[21] Y.H. Kim, E.D. Park, Appl. Catal. B: Environ. 96 (2010) 41–50.
[22] B. Li, C. Wang, G. Yi, H. Lin, Y. Yuan, Catal. Today 164 (2011) 74–79.
[23] R. Hu, C. Yan, L. Xie, Y. Cheng, D. Wang, Int. J. Hydrogen Energy 36 (2011) 64–71.
[24] M.P. Woods, P. Gawade, B. Tan, U.S. Ozkan, Appl. Catal. B: Environ. 97 (2010) 28–35.
[25] T. Caputo, L. Lisi, R. Pirone, G. Russo, Appl. Catal. A: Gen. 348 (2008) 42–53.
[26] Z. Wu, H. Zhu, Z. Qin, H. Wang, L. Huang, J. Wang, Appl. Catal. B: Environ. 98 (2010) 204–212.
[27] S. Lu, C. Zhang, Y. Liu, Int. J. Hydrogen Energy 36 (2011) 1939–1948.
[28] Z.K. Zhao, X.L. Lin, R.H. Jin, G.R. Wang, M.G. Qiu, Curr. Top. Catal. 9 (2010) 1–14.
[29] A.L. Cámara, A. Kubacka, Z. Schay, Zs. Koppány, A. Martínez-Arias, J. Power Sources 196 (2011) 4364–4369.
[30] C.R. Jung, A. Kundu, S.W. Nam, H. Lee, Appl. Catal. B: Environ. 84 (2008) 426–432.
[31] C. Gu, S. Lu, J. Miao, Y. Liu, Y. Wang, Int. J. Hydrogen Energy 35 (2010) 6113–6122.
[32] D. Gamarra, A. Martínez-Arias, J. Catal. 263 (2009) 189–195.
[33] G. Marbán, I. López, T. Valdés-Solís, A.B. Fuertes, Int. J. Hydrogen Energy 33 (2008) 6687–6695.
[34] Z. Yao, X. Zhang, F. Peng, H. Yu, H. Wang, J. Yang, Int. J. Hydrogen Energy 36 (2011) 1955–1959.
[35] M. Kang, M.W. Song, C.H. Lee, Appl. Catal. A: Gen. 251 (2003) 143–156.
[36] S. Sun, Q. Gao, H. Wang, J. Zhu, H. Guo, Appl. Catal. B: Environ. 97 (2010) 284–291.
[37] X.W. Xie, Y. Li, Z.Q. Liu, M. Haruta, W.J. Shen, Nature 458 (2009) 746–749.
[38] H.L. Li, X.H. Yu, S.T. Tu, J.Y. Yan, Z.D. Wang, Appl. Catal. A: Gen. 387 (2010) 215–223.
[39] K. Omata, Y. Kobayashi, M. Yamada, Catal. Commun. 8 (2007) 1–5.
[40] Z.K. Zhao, M.M. Yung, U.S. Ozkan, Catal. Commun. 9 (2008) 1465–1471.
[41] M.M. Yung, Z.K. Zhao, M.P. Woods, U.S. Ozkan, J. Mol. Catal. A: Chem. 279 (2008) 1–9.

[42] Y. Hasegawa, R. Maki, M. Sano, T. Miyake, Appl. Catal. A: Gen. 371 (2009) 67–72.
[43] J. Li, P. Zhu, S. Zuo, Q. Huang, R. Zhou, Appl. Catal. A: Gen. 381 (2010) 261–266.
[44] E.C. Njagi, H.C. Genuino, C.K. King'ondu, C. Chen, D. Horvath, S.L. Suib, Int. J. Hydrogen Energy 36 (2011) 6768–6779.
[45] Q. Zhang, X. Liu, W. Fan, Y. Wang, Appl. Catal. B: Environ. 102 (2011) 207–214.
[46] Q. Guo, S. Chen, Y. Liu, Y. Wang, Chem. Eng. J. 165 (2010) 846–850.
[47] K. Sirichaiprasert, A. Luengnaruemitchai, S. Pongstabodee, Int. J. Hydrogen Energy 32 (2007) 915–926.
[48] G. Zhou, Y. Jiang, H. Xie, F. Qiu, Chem. Eng. J. 109 (2005) 141–145.
[49] Z.K. Zhao, R.H. Jin, T. Bao, X.L. Lin, G.R. Wang, Appl. Catal. B: Environ. 110 (2011) 154–163.
[50] G. Avgouropoulos, T. Ioannides, Appl. Catal. A: Gen. 244 (2003) 155–167.
[51] J.L. Ayastuy, A. Gurbani, M.P. González-Marcos, M.A. Gutiérrez-Ortiz, Appl. Catal. A: Gen. 387 (2010) 119–128.
[52] S. Todorova, H. Kolev, J.P. Holgado, G. Kadinov, Ch. Bonev, R. Pereñíguez, A. Caballero, Appl. Catal. B: Environ. 94 (2010) 46–54.
[53] D. Li, X. Liu, Q. Zhang, Y. Wang, H. Wan, Catal. Lett. 127 (2009) 377–385.
[54] J. Villaseñor, P. Reyes, G. Pecchi, Catal. Today 76 (2002) 121–131.
[55] W.Y. Hernández, M.A. Centeno, F. Romero-Sarria, S. Ivanova, M. Montes, J.A. Odriozola, Catal. Today 157 (2010) 160–165.
[56] H.G. EI-Shobaky, M.A. Shouman, A.A. Attia, Colloids Surf. A 274 (2006) 62–70.
[57] F. Morales, E. de Smit, M.F. de Groot, T. Visser, B.M. Weckhuysen, J. Catal. 246 (2007) 91–99.
[58] J. Gao, J. Guo, D. Liang, Z. Hou, J. Fei, X. Zheng, Int. J. Hydrogen Energy 33 (2008) 5493–5500.
[59] A. Gómez-Cortés, Y. Márquez, J. Arenas-Alatorre, G. Díaz, Catal. Today 133–135 (2008) 743–749.
[60] J.W. Park, J.H. Jeong, W.L. Yoon, Y.W. Rhee, J. Power Sources 132 (2004) 18–28.